Intracranial Volume Quantification from 3D Photography

Liyun Tu[1(✉)], Antonio R. Porras[1], Scott Ensel[1], Deki Tsering[2], Beatriz Paniagua[3], Andinet Enquobahrie[3], Albert Oh[4], Robert Keating[2], Gary F. Rogers[4], and Marius George Linguraru[1,5]

[1] Sheikh Zayed Institute for Pediatric Surgical Innovation, Children's National Health System, Washington DC, USA
tuliyun@gmail.com
[2] Division of Neurosurgery, Children's National Health System, Washington DC, USA
[3] Kitware Inc., Carrboro, NC, USA
[4] Division of Plastic and Reconstructive Surgery, Children's National Health System, Washington DC, USA
[5] School of Medicine and Health Sciences, George Washington University, Washington DC, USA

Abstract. 3D photography offers non-invasive, radiation-free, and anesthetic-free evaluation of craniofacial morphology. However, intracranial volume (ICV) quantification is not possible with current non-invasive imaging systems in order to evaluate brain development in children with cranial pathology. The aim of this study is to develop an automated, radiation-free framework to estimate ICV. Pairs of computed tomography (CT) images and 3D photographs were aligned using registration. We used the real ICV calculated from the CTs and the head volumes from their corresponding 3D photographs to create a regression model. Then, a template 3D photograph was selected as a reference from the data, and a set of landmarks defining the cranial vault were detected automatically on that template. Given the 3D photograph of a new patient, it was registered to the template to estimate the cranial vault area. After obtaining the head volume, the regression model was then used to estimate the ICV. Experiments showed that our volume regression model predicted ICV from head volumes with an average error of 5.81 $\pm$ 3.07% and a correlation (R^2) of 0.96. We also demonstrated that our automated framework quantified ICV from 3D photography with an average error of 7.02 $\pm$ 7.76%, a correlation (R^2) of 0.94, and an average estimation error for the position of the cranial base landmarks of 11.39 $\pm$ 4.3 mm.

Keywords: 3D photography · Computed tomography · Intracranial volume quantification · Registration

1 Introduction

Cranial volume analysis is important to assess craniofacial development and pathology. Specifically, intracranial volume (ICV) plays an essential role in the assessment of craniosynostosis and the decision factors for treatment, since the early fusion of the

M.J. Cardoso et al. (Eds.): CARE/CLIP 2017, LNCS 10550, pp. 116–123, 2017.
DOI: 10.1007/978-3-319-67543-5_11

cranial sutures can alter brain growth [1, 2]. In addition, longitudinal assessment of ICV is equally important after surgical treatment to evaluate the outcome of the intervention.

Most methods to quantify ICV are based on brain segmentation from computed tomography (CT) [3] or magnetic resonance imaging (MRI) scans [4]. However, CT involves radiation and MRI typically requires sedation or anesthesia for young children. Due to concerns about the risks of radiation and/or sedation in these patients, 3D photography has become an increasingly attractive modality to assess head volume, since it offers radiation-free, non-invasive, and anesthetic-free imaging [5, 6].

Wilbrand et al. [7] demonstrated that 3D photography has great potential to track and quantify the clinical course of surgical correction of craniosynostosis. Meulstee et al. [8] used 3D photography to evaluate the cranial shape to identify craniosynostosis. Freudlsperger et al. [9] used 3D photography to capture pre- and post-operative scans of children with metopic craniosynostosis to compare head volume (HV) changes before and after surgery. However, these works focus on the head volume and shape, which do not measure the ICV (volume inside the cranial vault).

The aim of this study is to automatically quantify the ICV from 3D photography. First, we register a set of paired CT images and 3D photographs from the same patients to create a regression model that estimates the ICV (obtained from CT) from the HV measured from the 3D photography. We then use the regression model in conjunction with the 3D photograph of a new patient, for which we automatically measure the HV using registration to a 3D photograph reference template. The resulting framework allows us to automatically quantify the ICV from 3D photography to monitor patients with cranial pathology.

2 Materials and Methods

In the following sections, we will describe each component of our framework to fully automatic estimate ICV from 3D photography (see Fig. 1).

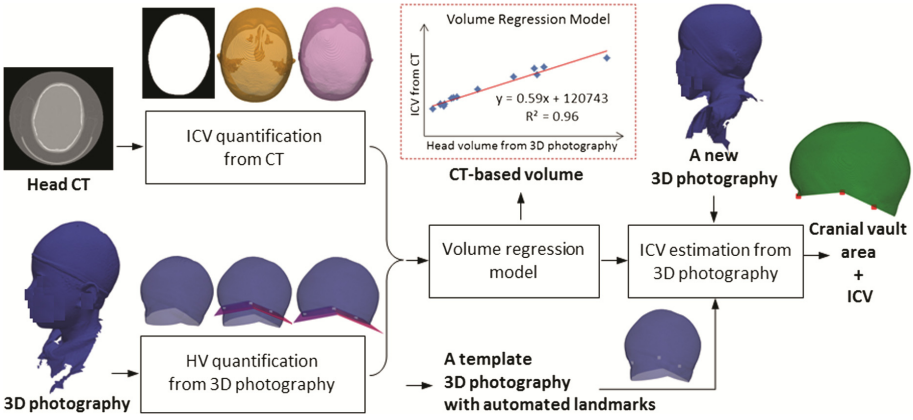

Fig. 1. Schematic of the proposed framework. ICV: intracranial volume. HV: head volume. The methods used for each of the boxes in this figure are detailed in Sect. 2 of the paper.

2.1 Data Description

Pairs of retrospective head CT imaging and 3D photography were collected by our institution from 14 subjects (average age 47 ± 66 months, range 2–199 months) with a variety of craniofacial pathologies (e.g., craniosynostosis and velopharyngeal insufficiency). All 3D photographs were taken at an average of 13 ± 18 days (range 0–49 days) from their corresponding CTs. CT image in-plane resolution ranged 0.26–0.49 mm, with axial spacing smaller or equal to 5 mm. 3D photographs were acquired using the 3dMDhead System (3dMD, Atlanta, GA). In the next sections, we will refer to this dataset as Φ_{pairs}.

In addition, we also collected an independent dataset Φ_{singles} of 3D photographs from 14 new patients (average age 88 ± 62 months, range 7–193 months) with craniofacial pathologies without paired CT.

2.2 Intracranial Volume Quantification from CT

To register a 3D photograph to its paired CT image (Φ_{pairs} dataset), we first created a 3D surface representing the patient's head (including the skin) from CT. We segmented the image areas with signal intensity higher than −200 Hounsfield units (HU), which separates the whole head from the background. We used morphological opening to isolate the inner tissues and we extracted the largest connected component, which provided a binary mask defining the patient's head. The marching cubes algorithm [10] was used to reconstruct the head surface from the image, which resulted in a single layered triangular mesh of the head.

The cranial bones were extracted from CT using the approach described in [3, 11]. In summary, a binary image with the bone structures was obtained from CT by thresholding at HU > 100. This binary image was then registered (optimizing translation, rotation and scaling) to a reference template in which a set of 4 landmarks were manually placed at the nasion, opisthion and the two clinoid processes of the dorsum sellae. This registration identified the location of these landmarks in the CT image of each patient, which define the two planes at the cranial base that we used to extract the cranial vault. Given the cranial vault of the patient, the CT-based intracranial volume (V_{CT_ICV}) was calculated as the volume within the cranial vault (i.e. between the cranial bones and the planes defined by the cranial base landmarks).

2.3 Head Volume Quantification from 3D Photography

To extract the part of the head surface obtained from 3D photography that corresponds to the cranial vault, the head surface obtained from its paired CT was registered to the 3D photograph using the iterative closest point algorithm (ICP) [12], which minimized the following equation:

$$E = \sum_{i=0}^{N} \left| Tp_i - q_i \right|^2, \tag{1}$$

where p_i are the homogeneous coordinates of point i in the head surface extracted from CT, q_i are corresponding coordinates in the 3D photograph, N is the number of points on the surface from CT, and T is the rigid transformation estimated. Point correspondences were established by searching each point on the CT surface to locate its closest point in the 3D photograph.

After registration, the cranial base landmarks identified in the CT image were propagated to the 3D photograph using T. The head volume (V_{3D_HV}) from the 3D photograph was calculated as the volume between the head surface and the cranial base defined by the 4 cranial base landmarks, as illustrated in Fig. 2.

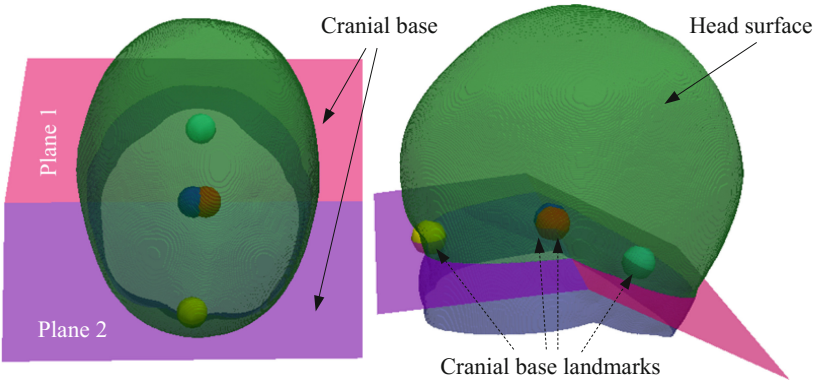

Fig. 2. Cranial vault area estimation for head volume measurement. The green surface represents the patient's head surface, which can be obtained from CT or 3D photograph. The cranial base (in purple) corresponds to two planes defined by the 4 cranial base landmarks at the nasion, opisthion and the two clinoid processes of the dorsum sellae. (Color figure online)

2.4 Intracranial Volume Estimation from 3D Photography

From the two volumes quantified in previous sections, V_{CT_ICV} and V_{3D_HV}, we built a linear regression model. This model will allow predicting the ICV given the HV calculated from the 3D photograph of a patient (V_{3D_HV}). In this section, we present a method to estimate V_{3D_HV} without the need of a paired CT image.

We selected a 3D photograph of a patient with a paired CT image as a reference template (R_{shape}) in which we located the cranial base landmarks ($R_{landmark}$) using its CT image as previously explained. Then, given the 3D photograph of a new patient (M_{shape}), we registered it to the reference template to estimate the location of the landmarks. Table 1 shows the proposed registration algorithm.

Table 1. Cranial base landmarks estimation via registration.

Input: R_{shape}, $R_{landmark}$, M_{shape}
Output: $M_{landmark}$
calculate an optimal affine transformation $\boldsymbol{T}_{\text{affine}}: (R_{shape}) \mapsto M_{shape}$
transform the landmark $M'_{landmark} = \boldsymbol{T}_{\text{affine}}: (R_{landmark})$
initialize the non-rigid transformation using $\boldsymbol{T}_{\text{affine}}(R_{shape})$
calculate an optimal B-splines based transformation, $\boldsymbol{T}_{\text{local}}: \boldsymbol{T}_{\text{affine}}(R_{shape}) \mapsto M_{shape}$
estimate the landmark $M_{landmark} = \boldsymbol{T}_{\text{local}}: (M'_{landmark})$

$\boldsymbol{T}_{\text{affine}}$ is an affine surface-based transformation estimated using the ICP algorithm, as shown in Eq. 1. $\boldsymbol{T}_{\text{local}}$ is a B-spline based transformation estimated as proposed in [13]. The registration between R_{shape} and M_{shape} is first optimized by affine transformation, and then refined by a non-rigid deformation.

This registration allows determining the position of the 4 cranial base landmarks on a new 3D photograph without using a corresponding CT image, and thus computing the HV. Using the volume regression model created in previous section, we then estimated the ICV from the calculated HV.

3 Evaluation and Results

The CT-based true intracranial volume (V_{CT_ICV}) and the head volume (V_{3D_HV}) from its corresponding 3D photograph in dataset Φ_{pairs} were computed to create a linear regression model as explained in Sect. 2.2. The model, which is shown in Fig. 3, yielded a clinically acceptable average volumetric error of $5.81 \pm 3.07\%$ and a correlation (R^2) of 0.96.

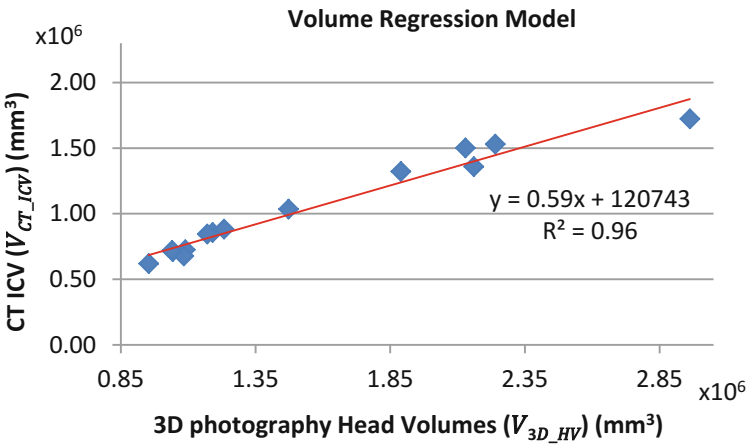

Fig. 3. Linear regression model predicting intracranial volume based on the automated head volume quantification from 3D photography.

We used the proposed framework to estimate the ICV (V_{3D_ICV}) using only the 3D photographs from the patients in Φ_{pairs}, and we compared the estimated values with the real ICV (V_{CT_ICV}) quantified from their paired CT images. We obtained an average volumetric error of $7.02 \pm 7.76\%$ and a correlation (R^2) of 0.94. In addition, we obtained an average estimation error for the position of the cranial base landmarks of 11.39 ± 4.3 mm. Figure 4 represents the Bland-Altman analysis [14] showing the agreement between V_{3D_ICV} and V_{CT_ICV}. There was one outlier that represents 31.67% of the error due to artifacts in the 3D photograph close to the neck area, which could be improved by a more efficient pre-processing. If we exclude this case the average volumetric error decreases to $5.16 \pm 3.63\%$. Next, we used a Wilcoxon rank-sum test to test whether the distribution of V_{3D_ICV} and V_{CT_ICV} were statistically different, obtaining a p-value of 0.91. Therefore, we could not reject the hypothesis that the ICV estimated from 3D photography has the same distribution than the true ICV estimated from CT imaging.

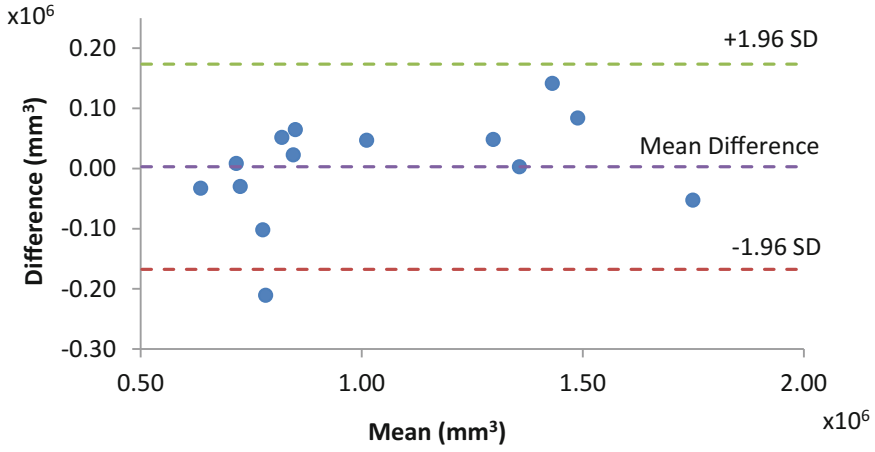

Fig. 4. Bland-Altman plot comparing the estimated ICV from 3D photography (V_{3D_ICV}) and the true ICV from CT (V_{CT_ICV}) for the patients in Φ_{pairs}.

Finally, we estimated the ICV from an independent dataset of 3D photographs ($\Phi_{singles}$) using the proposed framework. Figure 5 shows the ICV quantified from the 3D photographs of both datasets ($\Phi_{singles}$ and Φ_{pairs}) together with the true ICV from the CT images in Φ_{pairs}. We also calculated an age regression function of the form $y = \alpha x^{\beta}$ both for the true ICV volume from CT, and for the ICV estimated from 3D photography, where y is the ICV in mm^3 and x is the age of the patients in months. As it can be observed, the age regression functions are similar, indicating the potential to estimate ICV from 3D photography using our framework.

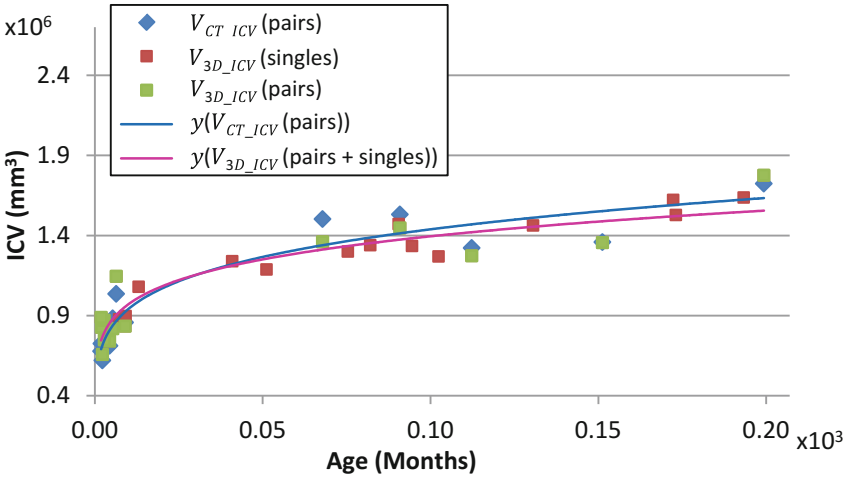

Fig. 5. Representation of the ICV against the age of the patients. Blue diamonds show the true ICV quantified from CT images for the cases from Φ_{pairs}. Green squares show the ICV estimated from 3D photography for the cases from Φ_{pairs}, while red squares show the ICV estimated from 3D photography for the cases in $\Phi_{singles}$. The blue line represents the age regression function estimated for the true ICV obtained from CT, while the magenta line represents the age regression function for the ICV estimated from 3D photography in both Φ_{pairs} and $\Phi_{singles}$. (Color figure online)

4 Conclusions

We proposed an automated, non-invasive, radiation-free framework to estimate intracranial volume (ICV) using 3D photography, and we evaluated its accuracy using CT-based measurements.

Experiments showed that our volume regression model predicted ICV from head volumes with an average error of $5.81 \pm 3.07\%$ and a correlation (R^2) of 0.96. We also demonstrated that our automated framework quantified ICV from 3D photography with an average error of $7.02 \pm 7.76\%$ (p-value = 0.91), a correlation (R^2) of 0.94, and an average estimation error for the position of the cranial base landmarks of 11.39 ± 4.3 mm.

Future work includes the validation of the proposed framework on a larger population. In addition, the framework can be extended to integrate cranial shape assessment, which will allow for a non-invasive longitudinal assessment of the surgical outcome for several craniofacial interventions.

Acknowledgements. This work was partly funded by the National Institutes of Health, Eunice Kennedy Shriver National Institute of Child Health and Human Development under grant NIH R42HD081712.

References

1. Anderson, P.J., Netherway, D.J., Abbott, A., David, D.J.: Intracranial volume measurement of metopic craniosynostosis. J. Craniofac. Surg. **15**(6), 1014–1016 (2004)
2. Paniagua, B., Emodi, O., Hill, J., Fishbaugh, J., Pimenta, L.A., Aylward, S.R., Andinet, E., Gerig, G., Gilmore, J., van Aalst, J.A., et al.: 3D of brain shape and volume after cranial vault remodeling surgery for craniosynostosis correction in infants. In: Proceeding of SPIE Medical Imaging, 2013, vol. 8672, p. 86720V (2013)
3. Mendoza, C.S., Safdar, N., Okada, K., Myers, E., Rogers, G.F., Linguraru, M.G.: Personalized assessment of craniosynostosis via statistical shape modeling. Med. Image Anal. **18**(4), 635–646 (2014)
4. Prastawa, M., Gilmore, J.H., Lin, W., Gerig, G.: Automatic segmentation of MR images of the developing newborn brain. Med. Image Anal. **9**(5), 457–466 (2005)
5. Ezaldein, H.H., Metzler, P., Persing, J.A., Steinbacher, D.M.: Three-dimensional orbital dysmorphology in metopic synostosis. J. Plast. Reconstr. Aesthetic Surg. **67**(7), 900–905 (2014)
6. Rodriguez-Florez, N., Göktekin, Ö.K., Bruse, J.L., Borghi, A., Angullia, F., Knoops, P.G., Tenhagen, M., O'Hara, J.L., Koudstaal, M.J., Schievano, S., et al.: Quantifying the effect of corrective surgery for trigonocephaly: a non-invasive, non-ionizing method using three-dimensional handheld scanning and statistical shape modeling. J. Cranio-Maxillofacial Surg. **45**(3), 387–394 (2017)
7. Wilbrand, J.-F., Szczukowski, A., Blecher, J.-C., Pons-Kuehnemann, J., Christophis, P., Howaldt, H.-P., Schaaf, H.: Objectification of cranial vault correction for craniosynostosis by three-dimensional photography. J. Cranio-Maxillofacial Surg. **40**(8), 726–730 (2012)
8. Meulstee, J.W., Verhamme, L.M., Borstlap, W.A., Van der Heijden, F., De Jong, G.A., Xi, T., Bergé, S.J., Delye, H., Maal, T.J.J.: A new method for three-dimensional evaluation of the cranial shape and the automatic identification of craniosynostosis using 3D stereophotogrammetry. Int. J. Oral Maxillofac. Surg. **46**(7), 819–826 (2017)
9. Freudlsperger, C., Steinmacher, S., Bächli, H., Somlo, E., Hoffmann, J., Engel, M.: Metopic synostosis: Measuring intracranial volume change following fronto-orbital advancement using three-dimensional photogrammetry. J. Cranio-Maxillofacial Surg. **43**(5), 593–598 (2015)
10. Lorensen, W.E., Cline, H.E.: Marching cubes: A high resolution 3D surface construction algorithm. Comput. Graph. (ACM) **21**(4), 163–169 (1987)
11. Porras, A.R., Zukic, D., Equobahrie, A., Rogers, G.F., Linguraru, M.G.: Personalized optimal planning for the surgical correction of metopic craniosynostosis. In: Shekhar, R., Wesarg, S., González Ballester, M.Á., Drechsler, K., Sato, Y., Erdt, M., Linguraru, M.G., Oyarzun Laura, C. (eds.) CLIP 2016. LNCS, vol. 9958, pp. 60–67. Springer, Cham (2016). doi: 10.1007/978-3-319-46472-5_8
12. Besl, P., McKay, N.: A method for registration of 3-D shapes. IEEE Trans. Pattern Anal. Mach. Intell. **14**(2), 239–256 (1992)
13. Rueckert, D., Sonoda, L.I., Hayes, C., Hill, D.L.G., Leach, M.O., Hawkes, D.J.: Nonrigid registration using free-form deformations: application to breast MR images. IEEE Trans. Med. Imaging **18**(8), 712–721 (1999)
14. Bland, J.M., Altman, D.: Statistical methods for assessing agreement between two methods of clinical measurement. Lancet **327**(8476), 307–310 (1986)